communications materials

ARTICLE

https://doi.org/10.1038/s43246-023-00378-z OPEN

Neon encapsulation by a hydroquinone organic crystalline clathrate under ambient conditions

Sol Geo Lim[1,7], Jong-Won Lee[2,7], Hiroshi Fujihisa[3,7], Chang Yeop Oh[1], Jiyeong Jang[1], Dohyun Moon[4], Satoshi Takeya[3], Michihiro Muraoka[5], Yoshitaka Yamamoto[5] & Ji-Ho Yoon[1,5,6]✉

The recent use of noble gases in laser devices and semiconductor lithography has greatly increased. However, there is no commercial technology for the storage of noble gases in solid materials owing to their chemical inertness and relative lightness. Here we report the simple synthesis and characteristics of a hydroquinone clathrate that stably captures neon at atmospheric pressure and room temperature. The highly flexible structure enables neon encapsulation in the one-dimensional channels of the clathrate framework despite their inter-cage migration through the hexagonal entrance of the cages. The neon uptake of as-synthesized hydroquinone clathrates is 37.3 g L^{-1} at 1 bar and 298 K. Increasing the temperature accelerates the release of neon from the flexible hydroquinone clathrate hydrogen-bonded organic framework, leading to guest-free clathrate formation at 1 bar and 400 K. This method represents a technological development for better storage and the controlled release of noble gases in solid structured materials.

[1] Department of Convergence Study on Ocean Science and Technology, Ocean Science and Technology (OST) School, Korea Maritime and Ocean University, Busan 49112, Korea. [2] Department of Environmental Engineering, Kongju National University, Chungnam 31080, Korea. [3] National Metrology Institute of Japan (NMIJ), National Institute of Advanced Industrial Science and Technology (AIST), Tsukuba, Ibaraki 305-8565, Japan. [4] Beamline Department, Pohang Accelerator Laboratory (PAL), Pohang 37673, Korea. [5] Energy Process Research Institute, AIST, Tsukuba, Ibaraki 305-8569, Japan. [6] Department of Energy and Resources Engineering, Korea Maritime and Ocean University, Busan 49112, Korea. [7] These authors contributed equally: Sol Geo Lim, Jong-Won Lee, Hiroshi Fujihisa. ✉email: jhyoon@kmou.ac.kr

Neon (Ne) is abundant on a universal scale because it is the fifth most abundant element in the universe after H, He, O, and C. However, Ne is relatively scarce on Earth and forms no compounds for immobilization in a solid, most likely due to its chemical inertness and relative lightness. Therefore, Ne is produced, transported, and stored only in a gas state despite its diverse range of use in industrial areas. Examples include in vacuum tubes, lighting devices, cryogenic refrigerants and red-light sources for helium-neon lasers. Particularly due to recent applications of Ne beams to semiconductor lithography, there is an increasing demand for Ne in commercial applications[1–3].

In general, Ne gas is produced from air via a cryogenic air separation process as a by-product of steel production. Ne is the second smallest noble gas after He, which has a kinetic diameter of 2.75 Å, slightly smaller than H_2 (2.89 Å)[4]. Therefore, it is very difficult to confine Ne in a cage structure. Thus far, there is no commercial technology for Ne storage in solid materials.

Clathrates are inclusion compounds formed by interactions between hosts and relatively light guest molecules captured in a variety type of cages. The stability of clathrate compounds primarily depends on the phase boundary in a temperature-pressure space, which is fundamentally caused by interactions between the host and guest molecules. Clathrate hydrates (gas hydrates) are a representative family of inclusion compounds and ice-like crystals containing gas (guest) molecules in hydrogen-bonded water (host) frameworks. In general, small gaseous guests such as CH_4, CO_2, and N_2 can be trapped in suitably sized cages of clathrates[5–9]. However, Ne and H_2 are too small to be stabilized in clathrate cages under moderate conditions. Thus, they form a crystalline clathrate structure that is typically stabilized under exceedingly high-pressure or low-temperature conditions. Regarding clathrate hydrates, H_2 molecules are captured in the small and large cages of the structure II clathrate hydrate in high-pressure conditions over 200 MPa[10,11]. It should be noted that Ne atoms require a higher pressure condition of 480 MPa at 260 K to construct ice II-structured Ne hydrates[12]. Unlike the filled-ice structure of Ne, a recent report demonstrated that the structure II (sII) hydrate can be synthesized with Ne by stepwise pressurization to a final pressure of 350 MPa at 244 K[13].

Organic clathrate is also a challenging material for gas storage, especially under ambient conditions. Hydroquinone (benzene-1,4-diol) has been recognized as a representative chemical for a host family of organic clathrates[8,9,14–17]. Hydroquinone clathrates form a hydrogen-bonded organic framework (HOF), capturing not only small guest molecules such as CH_4, CO_2, and N_2 but also relatively large hydrocarbons such as methanol, formic acid, and formamide. The intrinsically flexible and reversible hydrogen-bonding connections of HOFs[18,19] of hydroquinone clathrates endow to trap smaller gases such as H_2, He, and Ne. Similar to clathrate hydrates, hydroquinone forms a clathrate compound with H_2 molecules under a high-pressure condition of 200 MPa and 298 K to allow the crystallization of such HOFs by a gas-phase reaction[20]. However, H_2-loaded hydroquinone clathrates formed by gas-phase synthesis are not stable under ambient conditions when the pressure returns to atmospheric pressure. For Ne, no previous studies have reported organic clathrate compounds capturing Ne. From preliminary tests, we found that hydroquinone cannot form a clathrate structure with Ne through a gas-phase reaction at 150 MPa and room temperature.

Here, we show that Ne can form a clathrate structure with hydroquinone host molecules by recrystallization in ethanol with the help of resorcinol (benzene-1,3-diol). Surprisingly, Ne-loaded hydroquinone (Ne−hydroquinone) clathrates are stable under a completely ambient condition of 1 bar and 298 K. To the best of our knowledge, this Ne−hydroquinone clathrate is the first example of a clathrate compound capturing Ne under ambient conditions. The combined results using high-resolution synchrotron X-ray diffraction (XRD), solid-state ^{13}C cross-polarization magic-angle spinning (CPMAS) NMR, Raman spectroscopy, scanning electron microscopy (SEM), high-angle annular dark-field scanning transmission electron microscopy (HAADF-STEM), transmission electron microscopy (TEM), temperature-dependent synchrotron XRD, Rietveld refinement, Fourier difference mapping, molecular dynamics (MD) simulations, and density functional theory (DFT) calculations enable us to provide deeper insight related to gas storage in solid materials under ambient conditions.

Results

Formation and Ne storage capacity of Ne−hydroquinone clathrates. Ne−hydroquinone clathrates were synthesized in super-saturated ethanol solutions containing hydroquinone and resorcinol at a molar ratio of hydroquinone : resorcinol = 6 : 4 at 10 MPa of Ne gas. After a reaction for two days at −20 °C, recrystallized white solid materials were produced by decreasing the system pressure to ambient conditions, with a subsequent filtering step to separate the solid products from the ethanol solution in each case, followed by immediately drying under cold-air conditions (<20 °C). The molar ratio of 6 : 4 (hydroquinone : resorcinol) allows us to obtain the best high-yield production of Ne−hydroquinone clathrates by this recrystallization process when compared to other molar ratios. At first glance, it appears that these products are stable at room temperature and atmospheric pressure. SEM images show that the as-synthesized Ne−hydroquinone clathrate crystals have a mostly columnar or hexagonal prismatic shape with a length of <500 μm (Fig. 1a, b), in contrast to the needle-like crystal structures normally observed during the recrystallization of hydroquinone clathrates[16,17]. Similar to pure α-form hydroquinone (α-hydroquinone) crystals, the surface morphology of Ne−hydroquinone clathrate crystals is relatively clean and flat, different from other hydroquinone clathrates produced by gas-phase synthesis, which show porous surface roughness (Fig. 1b, c)[21,22]. The high-resolution synchrotron XRD pattern clearly indicates that the Ne−hydroquinone clathrates show a β-form hydroquinone (β-hydroquinone) structure with minute amounts (<2%) of α-hydroquinone and resorcinol (Fig. 1d). The lattice parameters of the Ne−hydroquinone clathrates are $a = 16.5604(3)$ Å and $c = 5.4788(6)$ Å with a space group of $R\bar{3}$ in the hexagonal dimensions. These values are reasonable for the β-hydroquinone clathrate structure and are comparable to those of CO_2−hydroquinone and CH_4−hydroquinone clathrates[23–25]. The Raman spectra of the Ne−hydroquinone clathrates show a single Raman peak at 1160 cm^{-1} and triplet features around 1600 cm^{-1}, indicating the formation of a β-hydroquinone clathrate (Fig. 1e)[23,24]. In addition, the solid-state ^{13}C CPMAS NMR spectra define the hydrogen-bonding characteristics of the Ne−hydroquinone clathrates, showing a singlet resonance peak at 148.6 ppm and a doublet peak at 118.2 and 116.3 ppm (Fig. 1f)[23,26]. To our surprise, there were no indications of the presence of resorcinol footprints, consistent with the XRD and Raman results. This indicates that resorcinol does not participate in clathrate formations as a host molecule. Overall, the combined results from XRD, Raman spectroscopy, and solid-state NMR enable us to confirm the formation of Ne−hydroquinone clathrate in a β-hydroquinone clathrate structure consisting of only hydroquinone molecules. As mentioned above, the molar ratio of 6 : 4 (hydroquinone : resorcinol) during the recrystallization process gives the best high-yield production of Ne−hydroquinone clathrates, despite the fact that they are constructed only with hydroquinone molecules. Therefore, we conjecture that resorcinol

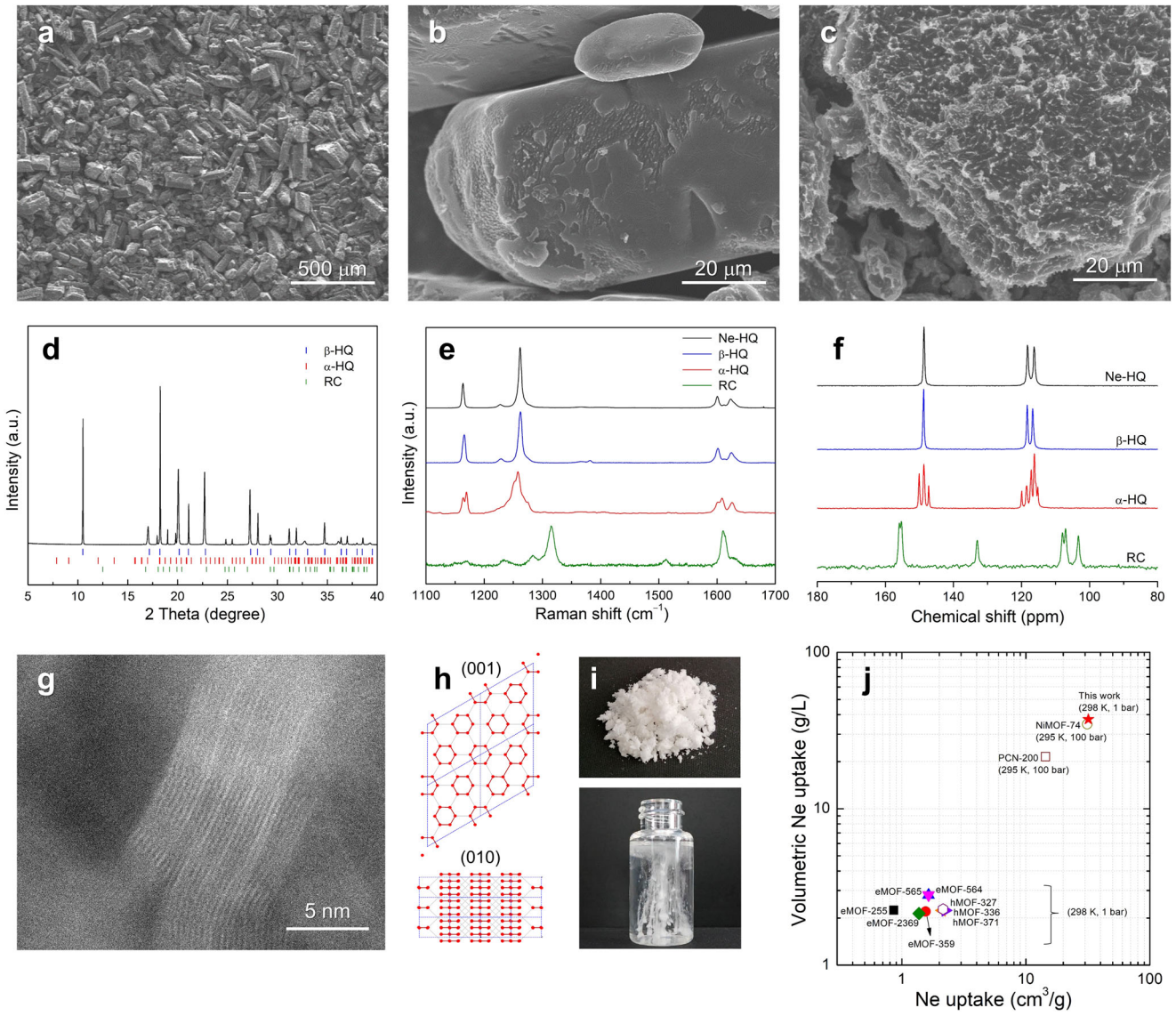

Fig. 1 Formation and characterization of Ne−hydroquinone clathrate. a, **b** FE-SEM images of Ne−hydroquinone clathrate. **c** FE-SEM image of Ar−hydroquinone clathrate synthesized by the gas-phase reaction. **d** High-resolution synchrotron XRD pattern of Ne−hydroquinone clathrate. **e** Raman and (**f**) solid-state ^{13}C CPMAS NMR spectra of Ne−hydroquinone clathrate, β-hydroquinone, α-hydroquinone, and resorcinol. **g** HAADF-STEM image of Ne−hydroquinone clathrate. **h** Hydrogen-bonding structure of Ne−hydroquinone clathrate shown along the (001) and (010) directions. O atoms of hydroquinone molecule are represented as red spheres. Thick red lines between O atoms represent hydrogen-bonding. Hydroquinone molecule is simplified with a longer thin gray line along the O−O axis of hydroquinone molecule for clarity and Ne guest molecules in the cages are omitted for clarity. Blue dashed lines are the unit cell. **i** Photographs of as-synthesized Ne−hydroquinone clathrates and Ne release from Ne−hydroquinone clathrate in ethanol (Supplementary Movies 1 and 2). **j** Comparison of Ne storage capacity of Ne−hydroquinone clathrate and MOFs[27–30]. Ne-HQ, β-HQ, α-HQ, and RC in **d**–**f** represent Ne−hydroquinone, β-hydroquinone, α-hydroquinone, and resorcinol, respectively.

plays an important role in the formation of Ne−hydroquinone clathrates as a template material to stabilize their structure but does not participate in the crystallization step. The HAADF-STEM image illustrates that the Ne−hydroquinone clathrates have flexible channel structures possessing curved 1D cage channels with tiny stripes (Fig. 1g). In the β-hydroquinone clathrate structure, the 1D cage channels are connected in the *c*-axis direction via hydrogen-bonded hexagons surrounded by six hydroquinone molecules, providing a facile route for Ne migration (Fig. 1h). Surprisingly, as mentioned above, these Ne−hydroquinone clathrates are stable under ambient conditions despite the fact that they capture noticeable amounts of Ne (Fig. 1i and Supplementary Movies 1 and 2).

The Ne storage capacity of the Ne−hydroquinone clathrates was determined by gravimetric measurements after the Ne was released from the as-synthesized Ne−hydroquinone clathrates. The total amount of Ne captured in the cages of the Ne−hydroquinone clathrates at 1 bar and 298 K is estimated to be 31.9 $cm^3\ g^{-1}$ in the STP condition. This value is equivalent to 37.3 $g\,L^{-1}$ in volumetric units, which is more than ten times greater than the volumetric Ne uptake of metal-organic frameworks (MOFs) at 1 bar and 298 K, such as eMOF-564 (2.81 $g\,L^{-1}$) and hMOF-371 (2.28 $g\,L^{-1}$), outperforming other MOFs under high-pressure conditions, such as PCN-200 (21.5 $g\,L^{-1}$) and NiMOF-74 (34.7 $g\,L^{-1}$) at 100 bar and 295 K (Fig. 1j)[27–30]. Assuming that Ne atoms singly occupy the cages of β-

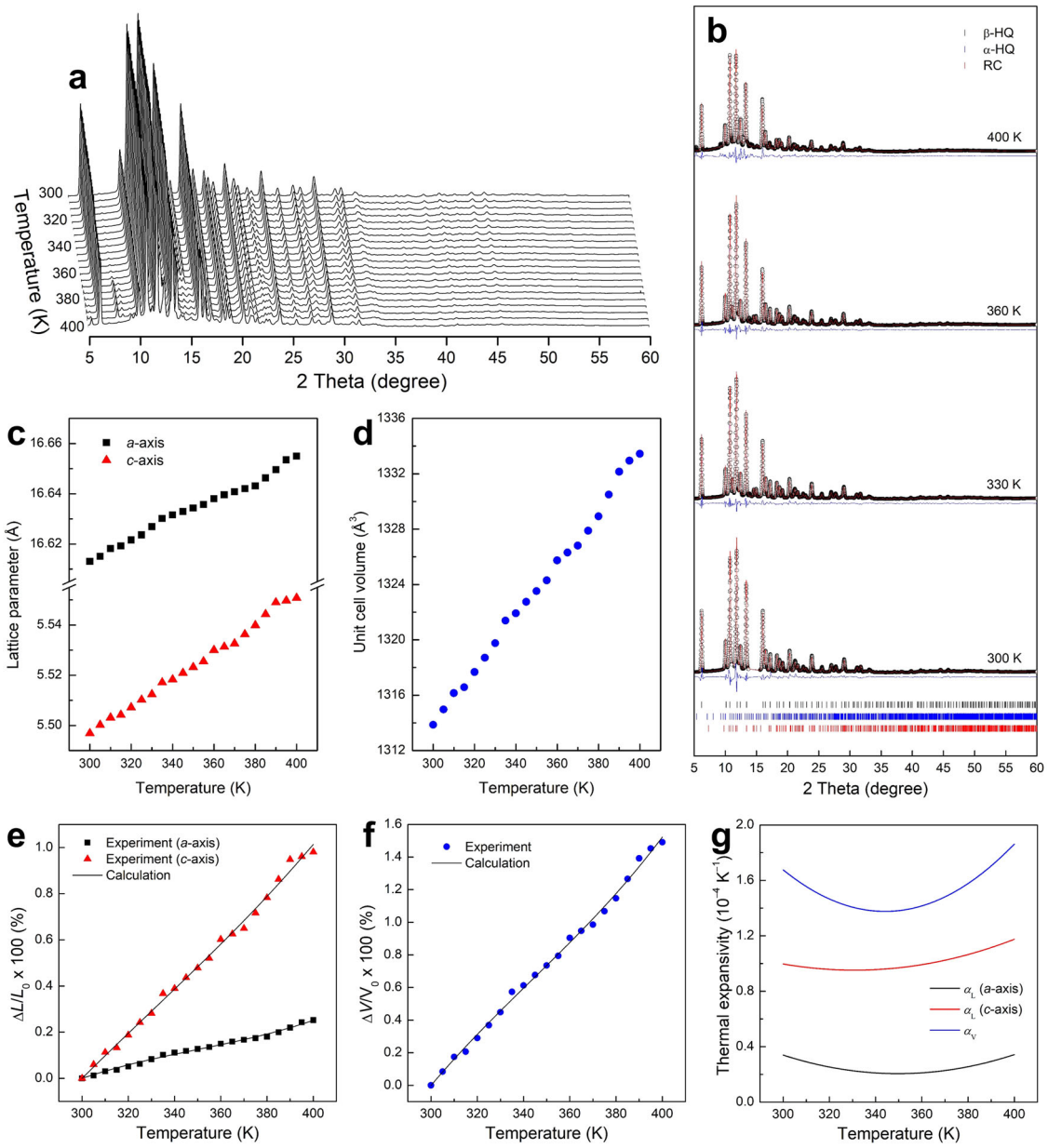

Fig. 2 XRD and thermal expansion of Ne−hydroquinone clathrate. a Temperature-dependent synchrotron XRD patterns of Ne−hydroquinone clathrate. **b** Rietveld refinements of selected XRD patterns of Ne−hydroquinone clathrate. Open black circle symbols are the observed patterns and red lines are the calculated patterns. Blue lines are differences between the observed and calculated patterns. β-HQ, α-HQ, and RC represent β-hydroquinone, α-hydroquinone, and resorcinol, respectively. **c** Lattice parameters and (**d**) unit cell volume of Ne−hydroquinone clathrate as a function of temperature. **e** Linear thermal expansion of Ne−hydroquinone clathrate along the *a*-axis and *c*-axis directions. **f** Volumetric thermal expansion of Ne−hydroquinone clathrate. **g** Thermal expansion coefficients of Ne−hydroquinone clathrate as a function of temperature.

hydroquinone clathrate, the cage occupancy of Ne−hydroquinone clathrates is calculated to $\theta = 0.47$ with the chemical formula of 0.47Ne·3hydroquinone, which is lower than CH_4−hydroquinone ($\theta = 0.69$) and CO_2−hydroquinone ($\theta = 0.74$) clathrates synthesized by the gas-phase reaction[23,24].

Thermal expansion properties and structural stability. Next, we focus on how Ne atoms are encapsulated in the cages of Ne−hydroquinone clathrates, and on the relationship between their structural stability and the occupancy of Ne atoms. Clearly, the temperature-dependent XRD patterns of Ne−hydroquinone clathrates show that there are no structural transformations caused by the increase in the temperature (Fig. 2a); therefore, they retain the β-hydroquinone clathrate structure at temperatures of 300–400 K, in contrast to other β-hydroquinone clathrates, such as Ar−hydroquinone and CH_4−hydroquinone clathrates, which show a structural transformation at 350–380 K[22,23]. In addition, the Rietveld refinement result indicates that the lattice parameters of the Ne−hydroquinone clathrate gradually increase with an increase in the temperature, resulting in a progressive thermal expansion of the unit cell volume (Fig. 2b–d). The typical anisotropic thermal expansion of Ne−hydroquinone clathrates is observed, as commonly found in organic crystal structures. The linear thermal expansion on the *c*-axis is approximately 1% in the temperature range of 300–400 K, while the lattice parameter *a* is expanded by ~0.2% (Fig. 2e). These linear expansions are equivalent to a volume expansion of ~1.5% (Fig. 2f). For all linear and volumetric expansions, the thermal expansion coefficients of

the Ne−hydroquinone clathrates follow a convex curve with a minimum point around 350 K as the temperature rises (Fig. 2g). This tendency may be closely related to changes in the cage occupancy of the Ne atoms in the hydroquinone clathrate framework accompanied by the increased temperature.

Ne encapsulation characteristics. To gain further insight into the occupation and migration behavior of Ne atoms in the cages of the Ne−hydroquinone clathrates, we undertook a combined examination of Rietveld refinement, Fourier difference mapping, and MD simulations. The Rietveld refinement results show that Ne atoms occupy the cage center in the HOFs of the β-hydroquinone clathrate structure with a cage occupancy of $\theta = 0.191$ (Fig. 3a and Supplementary Table 1). This estimated cage occupancy is significantly lower than the experimental value determined by the gravimetric measurements. Furthermore, the atomic displacement parameter of Ne is calculated and found to be $B_{iso} = 47.65$ Å^2, a considerably large value compared to those of other guest molecules[22,23]. This implies that Ne atoms reveal a large anisotropic displacement and/or highly disordered configuration in the cages of Ne−hydroquinone clathrates. In fact, Ne atoms may have substantial freedom in the cages of the hydroquinone clathrate framework because there is no chemical interaction or hydrogen-bonding between the guest Ne and host hydroquinone. In addition to their chemical inertness, the kinetic diameter of Ne atoms is substantially small, which allows them to migrate freely in the cages and 1D cage channels. The Fourier difference map of Ne−hydroquinone clathrates (Fig. 3b) shows that a strong site for guests is observed at the cage center, confirming the occupation of Ne atoms at the cage center. Interestingly, there is also a slightly disordered configuration that shows six possible positions around near the cage center. Together, these six positions form a hexagonal geometry with an edge length of ~1.4 Å, which is equivalent to the distance from the cage center. Nevertheless, the off-centered hexagonal positions are energetically unstable because the energy level of the hexagonal positions as determined by DFT calculations is higher than that of the cage center ($\Delta E = 0.1$–0.5 eV) (Supplementary Fig. 1). Consequently, these results indicate that the most favorable site for Ne atoms in Ne−hydroquinone clathrates is the cage center in the 1D channels. The dynamic effects of Ne as discussed here may have resulted in the apparently small cage occupancy value for Ne as determined by the Rietveld method.

MD simulations for Ne migration. Recent studies on MD simulations allow us to comprehensively investigate the structural properties of clathrate compounds encapsulating guest species[31–33]. In the hydroquinone clathrate framework, the mobility of guest molecules significantly depends on the molecular size of the guests. For hydroquinone clathrates containing CO_2 and CH_4 molecules[23–25], their molecular size is smaller than the internal size of the cage but larger than the hexagonal entrance in the HOFs of hydroquinone clathrates, which allows us to anticipate a guest immobilized in a cage. However, the cage flexibility of the hydroquinone clathrate framework enables some large guests to migrate in a cage-to-cage manner via the opening of the hexagonal entrances by the pore-widening process[22,24]. In contrast to the migration of these large guests, MD simulations show that Ne atoms are small enough to migrate freely in the cages and 1D channels of the hydroquinone clathrate framework without any structural alterations (Fig. 3c). It is also clearly shown that the most stable position for Ne atoms in the cages is the cage center. Thus, the movement of Ne in a cage is restricted to a confined space around the cage center. The maximum displacement of Ne atoms from the cage center on the *ab*-plane is approximately 1.8 Å (Fig. 3c and Supplementary Movie 3), slightly wider than the energetically local minimum positions estimated by the Fourier difference map. In contrast to the restricted displacement of Ne atoms on the *ab*-plane, for diffusion of Ne atoms along the *c*-axis, we observe and confirm the inter-cage migration of Ne atoms across the hexagonal entrance in Ne−hydroquinone clathrates (Fig. 3c and Supplementary Movie 4). The mean square displacements (MSDs) of Ne atoms along the *c*-axis are linearly fit to a time scale of approximately 400 ps (Supplementary Fig. 2), which is governed by the Einstein relationship for 1D diffusion[34,35],

$$<x^2(t)> = 2Dt \quad (1)$$

where D and t are the diffusion coefficient and the observation time, respectively, and $<x^2(t)>$ is the MSD of a particle. Based on Eq. (1) and Supplementary Fig. 2, the diffusion coefficient of Ne atoms in Ne−hydroquinone clathrates at 300 K is estimated as $D = 6.95 \times 10^{-10}$ m^2 s^{-1}. This value is smaller than the self-diffusion of Ne in water ($D = 4.18 \times 10^{-9}$ m^2 s^{-1} at 298 K)[36] but roughly two orders of magnitude larger than the diffusion coefficient of H_2 molecules in hydroquinone clathrate framework ($D = 8.49 \times 10^{-12}$ m^2 s^{-1} at 300 K)[37]. Evidently, this is due to the chemical inertness and smaller kinetic diameter of the Ne atoms.

Flexible structure for Ne storage under ambient conditions. Importantly, the TEM and HAADF-STEM images demonstrate high flexibility of the hydroquinone clathrates, possessing curved, bending, and in some cases 'scrambled' connections of the ID channels in the HOFs (Fig. 1g and 4a, b and Supplementary Fig. 3). From these results, we speculate that the distorted flexible structures of hydroquinone clathrates obstruct the migration of Ne atoms in the 1D channels, as shown in the MD simulations (Fig. 3c), meaning that the passing of Ne atoms is forbidden due to steric restrictions. As a result, Ne atoms cannot escape from the 1D channels in hydroquinone clathrates and are thus encapsulated in solid hydroquinone clathrate matrixes, even under the completely ambient condition of 1 bar and 298 K. It should be noted that the Ne−hydroquinone clathrate is the first example of a clathrate compound capturing Ne under ambient conditions. Notably, we also found that increasing the temperature accelerates the release of Ne from the HOFs of Ne−hydroquinone clathrates, eventually leading to the formation of a guest-free empty clathrate at 400 K, rarely observed in clathrate materials[13,38] (Fig. 4c). This is most likely due to the enhanced flexibility of the hydroquinone clathrates and the high diffusivity of Ne atoms in the 1D channels of the hydroquinone clathrates under the high-temperature conditions observed here (Fig. 4d).

Discussion

We have observed that Ne atoms can be captured in an organic clathrate structure, particularly under ambient conditions. Ne−hydroquinone clathrates were synthesized by recrystallization in ethanol with resorcinol as a template material and characterized using synchrotron XRD, Raman spectroscopy, SEM, TEM, STEM, and solid-state ^{13}C CPMAS NMR. The temperature-dependent XRD patterns showed no structural transformations upon an increase in the temperature, indicating that the Ne−hydroquinone clathrates retain the β-hydroquinone clathrate structure up to 400 K. The combined results of Rietveld refinement, Fourier difference mapping, DFT calculations, and MD simulations demonstrated that Ne atoms preferentially occupy the central position in the cages in Ne−hydroquinone clathrates, but they migrate freely via a cage-to-cage process through the hexagon entrance in the 1D channels of the hydroquinone clathrate framework. However, the highly flexible characteristics

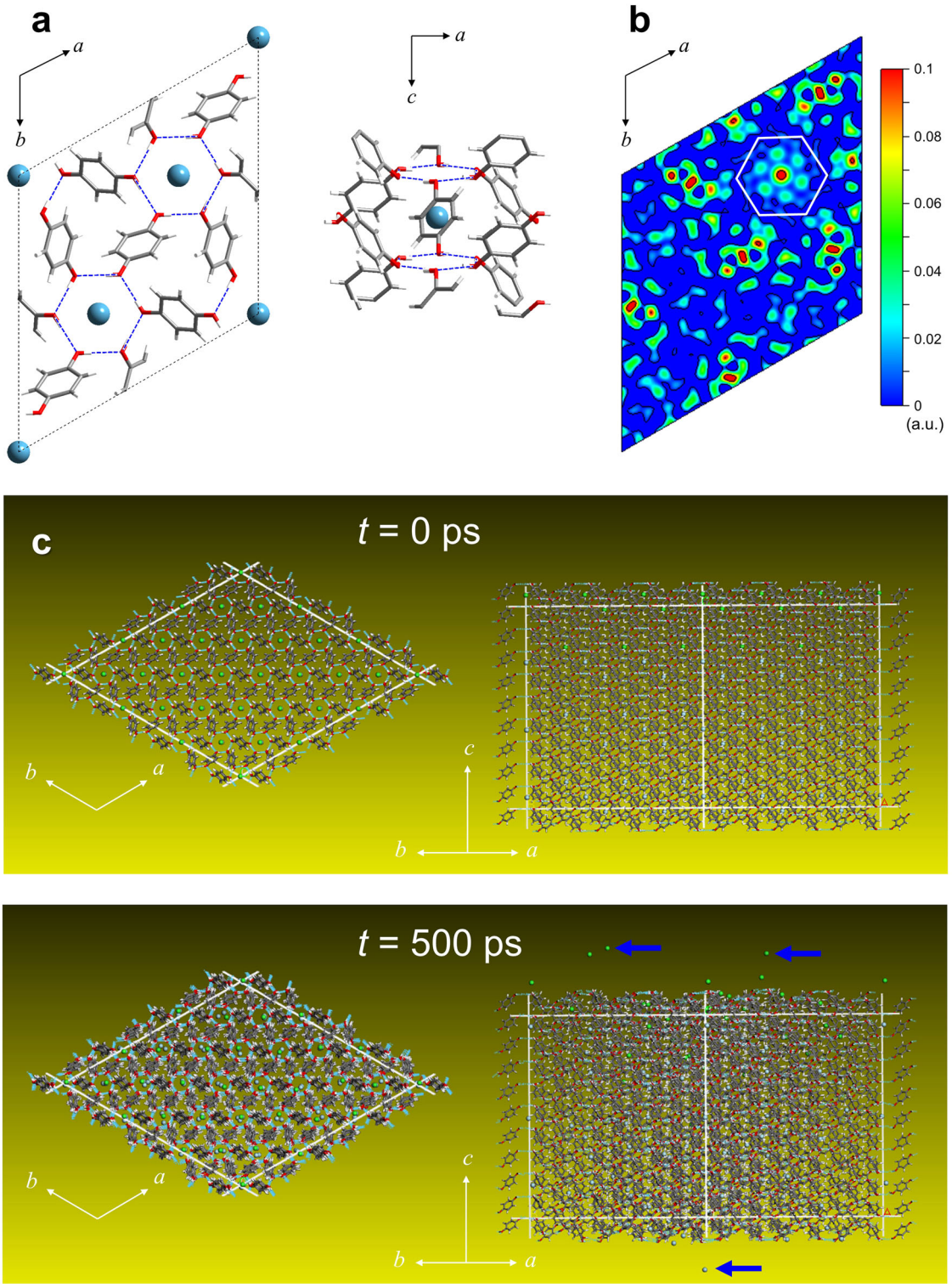

Fig. 3 Cage occupation behavior of Ne atoms in Ne–hydroquinone clathrate. a Cage structures of Ne–hydroquinone clathrate, viewed in the (001) direction. C, O, and H atoms are represented in gray, red, and white capped-sticks, respectively, and Ne atoms are represented in light blue spheres. Dotted black lines define a unit cell. Dashed blue lines represent hydrogen-bonding in the hexagonal cage entrance. Enlarged cage structure viewed along the (010) direction. **b** Fourier difference map of Ne–hydroquinone clathrate frameworks sliced at the cage center along the (001) plane. A white hexagon representing the hexagonal cage entrance is guide for the eye. **c** Snapshots from MD simulations for storage and migration of Ne atoms in the 3 × 3 × 9 supercell at 0 ps and 500 ps, viewed along the *ab*-plane and *c*-axis directions (Supplementary Movies 3 and 4). Some Ne atoms are colored in green for easy identification. Blue arrows at the snapshot indicate Ne atoms released from the supercell by diffusion.

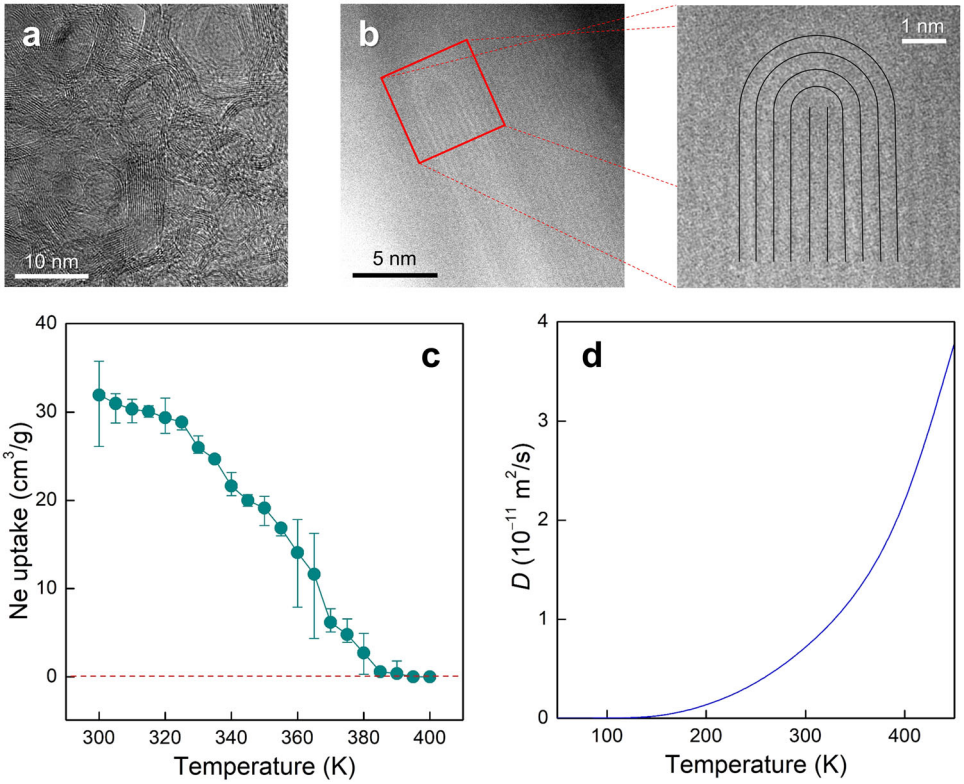

Fig. 4 Flexibility and Ne storage of hydroquinone clathrate. a TEM and (**b**) HAADF-STEM images of Ne−hydroquinone clathrate. Black lines are guide for the eye. **c** Ne uptake of Ne−hydroquinone clathrate as a function of temperature. **d** Diffusion coefficients of Ne atoms in Ne−hydroquinone clathrate calculated by MD simulations.

of hydroquinone clathrates allows the encapsulation of Ne atoms in the hydroquinone clathrate framework under ambient conditions. The Ne storage capacity of Ne−hydroquinone clathrates in an ambient condition was found to be much larger than that of MOFs. The effect of the temperature on the Ne uptake of Ne−hydroquinone clathrates was investigated to observe their structural stability and to determine the migration of Ne atoms in the HOFs of the Ne−hydroquinone clathrates. The complete release of Ne atoms without structural alterations facilitates the formation of a guest-free empty hydroquinone clathrate.

When solely hydroquinone was exposed to Ne gas in recrystallization, the resulting product of β-hydroquinone clathrates was unstable under ambient conditions and fully reverted to α-hydroquinone in two days. In this study, we introduce resorcinol as molecular templates to enhance the structural stability of β-hydroquinone clathrates. Even though the resorcinol molecules did not participate as a co-host in the clathrate framework, the Ne−hydroquinone clathrates formed in the presence of resorcinol exhibited a stable β-hydroquinone structure at the ambient condition of 298 K and 1 bar. Similar attempts to synthesize Ne−hydroquinone clathrates in the presence of catechol (benzene-1,2-diol) and phloroglucinol (benzene-1,3,5-triol) were unsuccessful. This indicates that resorcinol plays an important role in the formation of stable β-hydroquinone clathrates capturing Ne at ambient conditions.

The transition state (TS) for the inter-cage migration of Ne atoms was computed by the DFT calculations in $1 \times 1 \times 2$ supercell (Supplementary Fig. 4). The relaxation characteristics of hydrogen bonds in the hexagonal entrances built by six hydroquinone molecules was carefully considered in this model. The energy barrier, which is required for cage-to-cage movement of one Ne atom, obtained from the TS-search result was estimated to be 0.358 eV. Assuming that two Ne atoms are placed in a single cage (double occupancy), we found that the energy increased by 0.187 eV higher than single occupancy. Note that the energy difference between single and double occupancy of Ne is lower than the energy barrier for the inter-cage migration of Ne. This implies that double occupancy of Ne atoms in the cages of hydroquinone clathrates is a possible event. Nevertheless, we did not find any doubly-occupied cages by Ne atoms in the MD simulations with the initial cage occupancy of 1/3. However, much higher pressure conditions than 1 bar may allow us to anticipate double or triple cage occupancy of Ne atoms in hydroquinone clathrates, indicating a higher storage capacity of Ne in clathrate structures.

Methods

Synthesis of hydroquinone clathrates. Pure α-hydroquinone and resorcinol with a purity of 99.9 + % were purchased from Sigma-Aldrich and used without further purifications. A mixed powder of α-hydroquinone and resorcinol in a molar ratio of 6 :4 was dissolved and supersaturated in an ethanol solution. A high-pressure cell was used to expose the supersaturated ethanol solution to Ne gas at 10 MPa. The cell containing the ethanol solution and high-pressure guests was kept in a refrigerator at −20 °C for 48 h. The white crystals were obtained by opening the cell after a rapid depressurization step. The crystalline products were quickly poured on filter papers and dried to remove ethanol on the surface of the samples. The morphology of as-synthesized Ne–hydroquinone clathrates was observed by SEM and TEM/STEM systems equipped with a probe Cs corrector (JEM-ARM 200 F with Schottky type FEG operated at 200 kV equipped with CEOS Cs-corrector).

Synchrotron XRD. High-resolution synchrotron XRD measurements were carried out at the 9B beamline using a double-crystal Si(111) monochromator with a wavelength of 1.5176 Å at the Pohang Accelerator Laboratory (PAL). The diffraction patterns were obtained at an interval of 0.01° in the range of 5–130° under a vacuum condition. Temperature-dependent XRD diffraction data were collected using Debye-Scherrer rings with 66 mm of detector distance in 3 s exposure and a Rayonix MX225HS CCD area detector with synchrotron radiation ($\lambda = 0.9000$ Å) at the 2D SMC beamline at PAL. The PAL BL2D-SMC program was used for data collection, and the Fit2D program was used to convert 2D to 1D pattern[39].

Raman spectroscopy. A Raman spectrometer with a single-grating monochromator of 1800 grooves/mm, an air-cooled CCD detector, and a Nd:YAG laser (emitting 532 nm) with a power of 150 mW was used in this study.

Solid-state ^{13}C NMR spectroscopy. Solid-state NMR spectra were acquired using a 400 MHz spectrometer (Bruker Avance II^{+}) in a 9.4 T magnetic field. The ^{13}C NMR spectra were recorded at a Larmor frequency of 100.6 MHz. For the CPMAS spectra, a ^{1}H 90° pulse length of 3.9 µs, a contact time of 2 ms, a pulse repetition delay of 3 s, and proton decoupling were employed with a spinning rate of 10 kHz. The resonance peak of carbon atoms in adamantane was used as a chemical shift reference.

Gas storage capacity. The synthesized Ne−hydroquinone clathrate powders were placed in the bottom of a clean vial and some fine glass beads to prevent from sublimation of hydroquinone molecules during heating steps were also placed above the powder samples. To release Ne gases from hydroquinone clathrates, the vial containing hydroquinone clathrate samples and glass beads was heated on a hot plate at 80 °C. The heating steps were stopped when there is no mass change in the samples. The gas storage capacity of Ne−hydroquinone clathrates was determined by measuring changes in the sample mass after the release of gas from Ne −hydroquinone clathrates.

Thermal expansion coefficient. The volumetric thermal expansion coefficient represents the change in volume with temperature as[40,41]

$$\alpha_V = \frac{1}{V}\left(\frac{\partial V}{\partial T}\right)_P \tag{2}$$

Likewise, the uniaxial linear thermal expansion coefficient can be defined as the following equation.

$$\alpha_L = \frac{1}{L}\left(\frac{\partial L}{\partial T}\right)_P \tag{3}$$

The units of thermal expansion coefficients are in K^{-1}. When thermal expansion of materials is a function of temperature, the thermal expansion coefficients α (α_V and α_L) are determined by

$$\alpha = C_1 + C_2(T - T_0) + C_3(T - T_0)^2 \tag{4}$$

where T_0 is the reference temperature, 300 K in this study. Using Eqs. (2–4), the unit cell volume and lattice parameters of Ne−hydroquinone clathrates can be obtained by

$$\frac{V}{V_0} = \exp\left(C_1(T - T_0) + \frac{C_2}{2}(T - T_0)^2 + \frac{C_3}{3}(T - T_0)^3\right) \tag{5}$$

$$\frac{L}{L_0} = \exp\left(C_1(T - T_0) + \frac{C_2}{2}(T - T_0)^2 + \frac{C_3}{3}(T - T_0)^3\right) \tag{6}$$

where V is the unit cell volume and L is the lattice parameters, a and c. The coefficient parameters C_1, C_2, and C_3 can be obtained by fitting the equations to experimental results.

Rietveld refinement and Fourier difference map analysis. Rietveld refinements of XRD patterns were performed using the RIETAN program[42] and Fourier difference map was visualized by the VESTA program[43] with diffraction patterns and optimized atomic positions. Rigid-body constraints were used to fix the bond lengths, angles, and orientations in hydroquinone molecules. Only one B_{iso} parameter was calculated for C atoms.

MD simulation and DFT calculation. Classical MD simulations were performed using the BIOVIA Materials Studio (MS) Forcite Plus (version 2022 HF1)[44] with the COMPASS III force-field[45] and the Hoover-Nosé thermostat[46]. The force-filed parameters in the program were used without any adjustments. The $3 \times 3 \times 9$ supercell in the rhombohedral dimension and the NVT ensemble were used for a simulation time of 500 ps (1000000 points) with a time step of 0.5 fs. This system imposes periodic boundary conditions and contains 729 hydroquinone molecules. The cage occupancy of Ne in the hydroquinone clathrate frameworks was set to 1/3. In this case, the system contains 81 Ne atoms and thus totally 10,287 atoms. DFT calculations were performed using the CASTEP[47] with the generalized gradient approximation of Perdew-Burke-Ernzerhof functionals[48] and ultrasoft pseudopotentials[49] by employing the Tkatchenko-Scheffler dispersion correction[50]. The cutoff energy for the plane-wave was set to 630 eV. The Monkhorst-Pack grid separation[51] was set to approximately 0.07 Å^{-1}. The calculation of transition state for the inter-cage migration of Ne atoms was carried out using the CASTEP and the synchronous transit method[52] to estimate the energy barrier in $1 \times 1 \times 2$ supercell.

Data availability

The data that support the findings of this study have been included in the manuscript and Supplementary Information. Any additional data are available from the corresponding author upon reasonable request.

Received: 23 February 2023; Accepted: 26 June 2023;
Published online: 05 July 2023

References

1. Gonzalez, C. M. et al. Focused helium and neon ion beam induced etching for advanced extreme ultraviolet lithography mask repair. *J. Vac. Sci. Technol. B* **32**, 021602 (2014).
2. Stanford, M. G., Lewis, B. B. & Mahady, K. Review article: advanced nanoscale patterning and material synthesis with gas field helium and neon ion beams. *J. Vac. Sci. Technol. B* **35**, 030802 (2017).
3. Reisch, M. Noble gas shortages averted, for now. *C&EN Global Enterprise* **94**, 44 (2016).
4. Breck, D. W. *Zeolite in Molecular Sieves, Structure, Chemistry, and Use* (Wiley, 1974).
5. Sloan, E. D. & Koh, C. A. *Clathrate Hydrates of Natural Gases* (Taylor & Francis-CRC Press, 2008).
6. Berecz, E. & Bella-Achs, M. *Gas Hydrates* (Elsevier, 1983).
7. Sloan, E. D. Fundamental principles and applications of natural gas hydrates. *Nature* **426**, 353–359 (2003).
8. Palin, D. E. & Powell, H. M. Hydrogen bond linking of quinol molecules. *Nature* **156**, 334–335 (1945).
9. van der Waals, J. H. & Platteeuw, J. C. *Advances in Chemical Physics, Volume 2* (John Wiley & Sons, 1959).
10. Dyadin, Y. A. et al. Clathrate hydrates of hydrogen and neon. *Mendeleev Commun.* **9**, 209–210 (1999).
11. Mao, W. L. et al. Hydrogen clusters in clathrate hydrate. *Science* **297**, 2247–2249 (2002).
12. Yu, X. et al. Crystal structure and encapsulation dynamics of ice II-structured neon hydrate. *Proc. Natl. Acad. Sci. USA* **111**, 10456–10461 (2014).
13. Falenty, A., Hansen, T. C. & Kuhs, W. F. Formation and properties of ice XVI obtained by emptying a type sII clathrate hydrate. *Nature* **516**, 231–233 (2014).
14. Atwood, J. L., Davies, J. E. D. & MacNicol, D. D. *Inclusion compounds* (Academic Press, 1984).
15. Mock, J. E., Myers, J. E. & Trabant, E. A. Crystallization of the rare-gas clathrates. *Ind. Eng. Chem.* **53**, 1007–1010 (1961).
16. Palin, D. E. & Powell, H. M. The structure of molecular compounds. Part III. Crystal structure of addition complexes of quinol with certain volatile compounds. *J. Chem. Soc.* 208–221 (1947).
17. Powell, H. M. The structure of molecular compounds. Part IV. Clathrate compounds. *J. Chem. Soc.* 61–73 (1948).
18. Song, X. et al. Design rules of hydrogen-bonded organic frameworks with high chemical and thermal stabilities. *J. Am. Chem. Soc.* **144**, 10663–10687 (2022).
19. Lin, R.-B. & Chen, B. Hydrogen-bonded organic frameworks: chemistry and functions. *Chem* **8**, 2114–2135 (2022).
20. Strobel, T. A. et al. Chemical−clathrate hybrid hydrogen storage: storage in both guest and host. *J. Am. Chem. Soc.* **130**, 14975–14977 (2008).
21. Han, K. W. et al. Fast and reversible hydrogen storage in channel cages of hydroquinone clathrate. *Chem. Phys. Lett.* **546**, 120–124 (2012).
22. Woo, Y. et al. Extremely slow diffusion of argon atoms in clathrate cages: implications for gas storage in solid materials. *ACS Sustain. Chem. Eng.* **9**, 7479–7488 (2021).
23. Lee, J.-W. et al. Gas-phase synthesis and characterization of CH_4-loaded hydroquinone clathrates. *J. Phys. Chem. B* **114**, 3254–3258 (2010).
24. Lee, Y. J. et al. Selective CO_2 trapping in guest-free hydroquinone clathrate prepared by gas-phase synthesis. *ChemPhysChem* **12**, 1056–1059 (2011).
25. Coupan, R., Plantier, F., Torré, J.-P., Dicharry, C. & Sénéchal, P. Creating innovative composite materials to enhance the kinetics of CO_2 capture by hydroquinone clathrates. *Chem. Eng. J.* **325**, 35–48 (2017).
26. Ripmeester, J. A., Tse, J. S. & Davidson, D. W. ^{13}C NMR characterization of acetonitrile-hydroquinone clathrate. *Chem. Phys. Lett.* **86**, 428–433 (1982).
27. Guo, F., Liu, Y., Hu, J., Liu, H. & Hu, Y. Fast screening of porous materials for noble gas adsorption and separation: a classical density functional approach. *Phys. Chem. Chem. Phys.* **20**, 28193–28204 (2018).
28. Wood, P. A., Sarjeant, A. A., Yakovenko, A. A., Ward, S. C. & Groom, C. R. Capturing neon—the first experimental structure of neon trapped within a metal-organic environment. *Chem. Commun.* **52**, 10048–10051 (2016).
29. Wilmer, C. E. et al. Large-scale screening of hypothetical metal-organic frameworks. *Nat. Chem.* **4**, 83–89 (2012).
30. Liu, Y., Zhao, S., Liu, H. & Hu, Y. High-throughput and comprehensive prediction of H_2 adsorption in metal-organic frameworks under various conditions. *AIChE J.* **61**, 2951–2957 (2015).
31. Xu, K. et al. Structural and mechanical stability of clathrate hydrates encapsulating monoatomic guest species. *J. Mol. Liq.* **347**, 118391 (2022).

32. Liu, J. et al. Mechanical destabilization and cage transformations in water vacancy-contained CO_2 hydrates. *ACS Sustain. Chem. Eng.* **10**, 10339–10350 (2022).
33. Lin, Y. et al. Interfacial mechanical properties of tetrahydrofuran hydrate-solid surfaces: Implications for hydrate management. *J. Colloid Interface Sci.* **629**, 326–335 (2023).
34. Kärger, J., Ruthven, D. M. & Theodorou, D. N. *Diffusion in Nanoporous Materials*. (Wiley-VCH, 2012).
35. Gubbins, K. E., Liu, Y.-C., Moore, J. D. & Palmer, J. C. The role of molecular modeling in confined systems: impact and prospects. *Phys. Chem. Chem. Phys.* **13**, 58–85 (2011).
36. Holz, M., Haselmeier, R., Mazitov, R. K. & Weingartner, H. Self-diffusion of neon in water by ^{21}Ne NMR. *J. Am. Chem. Soc.* **116**, 801–802 (1994).
37. Pérez-Rodríguez, M., Otero-Fernández, J., Comesaña, A., Fernández-Fernández, Á. M. & Piñeiro, M. M. Simulation of capture and release processes of hydrogen by β-hydroquinone clathrate. *ACS Omega* **3**, 18771–18782 (2018).
38. Guloy, A. M. et al. A guest-free germanium clathrate. *Nature* **443**, 320–323 (2006).
39. Shin, J. W., Eom, K. & Moon, D. BL2D-SMC, the supramolecular crystallography beamline at the Pohang Light Source II, Korea. *J. Synchrotron Radiat.* **23**, 369–373 (2016).
40. Megaw, H. D. Crystal structures and thermal expansion. *Mater. Res. Bull.* **6**, 1007–1018 (1971).
41. Touloukian, Y. S. *Thermal expansion: nonmetallic solids*. (Plenum Publishing Corp., 1977).
42. Izumi, F. & Ikeda, T. A Rietveld-analysis program RIETAN-98 and its applications to zeolites. *Mater. Sci. Forum* **321-324**, 198–205 (2000).
43. Momma, K. & Izumi, F. VESTA 3 for three-dimensional visualization of crystal, volumetric and morphology data. *J. Appl. Cryst.* **44**, 1272–1276 (2011).
44. Dassault Systèmes Americas Corp., BIOVIA Materials Studio Forcite Plus Website, https://www.3ds.com/products-services/biovia/products/molecular-modeling-simulation/biovia-materials-studio/chemicals-solvents/ (accessed on 1 January 2023).
45. Akkermans, R. L. C. et al. COMPASS III: automated fitting workflows and extension to ionic liquids. *Mol. Simul.* **47**, 540–551 (2021).
46. Hoover, W. Canonical dynamics: equilibrium phase-space distributions. *Phys. Rev. A* **31**, 1695–1697 (1985).
47. Clark, S. J. et al. First principles methods using CASTEP. *Z. Kristallogr.* **220**, 567–570 (2005).
48. Perdew, J. P., Burke, K. & Ernzerhof, M. Generalized gradient approximation made simple. *Phys. Rev. Lett.* **77**, 3865–3868 (1996).
49. Vanderbilt, D. Soft self-consistent pseudopotentials in a generalized eigenvalue formalism. *Phys. Rev. B* **41**, 7892–7895 (1990).
50. Tkatchenko, A. & Scheffler, M. Accurate molecular van der Waals interactions from ground-state electron density and free-atom reference data. *Phys. Rev. Lett.* **102**, 073005 (2009).
51. Monkhorst, H. J. & Pack, J. D. Special points for Brillouin-zone integrations. *Phys. Rev. B* **13**, 5188–5192 (1976).
52. Govind, N., Petersen, M., Fitzgerald, G., King-Smith, D. & Andzelm, J. A generalized synchronous transit method for transition state location. *Comput. Mater. Sci.* **28**, 250–258 (2003).

Acknowledgements

We thank Dr. John A. Ripmeester for helpful discussions. Synchrotron XRD measurements were performed at the Pohang Accelerator Laboratory supported by the Ministry of Science and ICT (MSIT) and POSTECH. Solid-state NMR data were acquired at the Western Seoul Center of KBSI. This work was supported by the Mid-Career Research Program (2021R1A2C2010783) through National Research Foundation of Korea funded by MSIT.

Author contributions

J.-H.Y. conceived and designed the project. S.G.L., J.-W.L., C.Y.O., J.J. and D.M. conducted the experiments. H.F. performed the DFT and MD simulations. S.G.L., J.-W.L., H.F., S.T., M.M., Y.Y. and J.-H.Y. performed the interpretation of data. S.G.L. and J.-H.Y. wrote the manuscript with the help from all authors. All authors critically reviewed the manuscript.

Competing interests

The authors declare no competing interests.

Additional information

Supplementary information The online version contains supplementary material available at https://doi.org/10.1038/s43246-023-00378-z.

Correspondence and requests for materials should be addressed to Ji-Ho Yoon.

Peer review information *Communications Materials* thanks Shuanshi Fan, Jianyang Wu, Manuel Martínez Piñeiro and the other, anonymous, reviewer(s) for their contribution to the peer review of this work. Primary Handling Editors: Jet-Sing Lee. A peer review file is available.

Reprints and permission information is available at http://www.nature.com/reprints

Publisher's note Springer Nature remains neutral with regard to jurisdictional claims in published maps and institutional affiliations.